Am J Physiol Cell Physiol 316: C92–C103, 2019.
First published November 14, 2018; doi:10.1152/ajpcell.00346.2018.

RESEARCH ARTICLE

Piezo1 mediates angiogenesis through activation of MT1-MMP signaling

Hojin Kang,[1,2] Zhigang Hong,[1] Ming Zhong,[1] Jennifer Klomp,[1] Kayla J. Bayless,[3] Dolly Mehta,[1] Andrei V. Karginov,[1] Guochang Hu,[1,2]* and Asrar B. Malik[1]*

[1]*Department of Pharmacology and The Center for Lung and Vascular Biology, The University of Illinois College of Medicine, Chicago, Illinois;* [2]*Department of Anesthesiology, The University of Illinois College of Medicine, Chicago, Illinois; and* [3]*Department of Molecular and Cellular Medicine, Texas A&M University Health Science Center, College Station, Texas*

Submitted 29 August 2018; accepted in final form 7 November 2018

Kang H, Hong Z, Zhong M, Klomp J, Bayless KJ, Mehta D, Karginov AV, Hu G, Malik AB. Piezo1 mediates angiogenesis through activation of MT1-MMP signaling. *Am J Physiol Cell Physiol* 316: C92–C103, 2019. First published November 14, 2018; doi: 10.1152/ajpcell.00346.2018.—Angiogenesis is initiated in response to a variety of external cues, including mechanical and biochemical stimuli; however, the underlying signaling mechanisms remain unclear. Here, we investigated the proangiogenic role of the endothelial mechanosensor Piezo1. Genetic deletion and pharmacological inhibition of Piezo1 reduced endothelial sprouting and lumen formation induced by wall shear stress and proangiogenic mediator sphingosine 1-phosphate, whereas Piezo1 activation by selective Piezo1 activator Yoda1 enhanced sprouting angiogenesis. Similarly to wall shear stress, sphingosine 1-phosphate functioned by activating the Ca^{2+} gating function of Piezo1, which in turn signaled the activation of the matrix metalloproteinase-2 and membrane type 1 matrix metalloproteinase during sprouting angiogenesis. Studies in mice in which Piezo1 was conditionally deleted in endothelial cells demonstrated the requisite role of sphingosine 1-phosphate-dependent activation of Piezo1 in mediating angiogenesis in vivo. These results taken together suggest that both mechanical and biochemical stimuli trigger Piezo1-mediated Ca^{2+} influx and thereby activate matrix metalloproteinase-2 and membrane type 1 matrix metalloproteinase and synergistically facilitate sprouting angiogenesis.

angiogenesis; endothelium; mechanosensor; Piezo1; wall shear stress

INTRODUCTION

Angiogenesis, the formation of new capillaries from preexisting vessels, is an essential feature of embryonic development, inflammation, wound healing, tissue repair, and tumor growth (3). Stages of angiogenesis include transition of quiescent endothelial cells (ECs) to the active phenotype followed by degradation of extracellular matrix (ECM) proteins due to the activation of metalloproteinases that leads to sprouting of new vessels in the provisional ECM (36). Release of proangiogenic factors such as sphingosine 1-phosphate (S1P), vascular endothelial growth factor (VEGF), and basic fibroblast growth factor as well as mechanical stimuli such as wall shear stress (WSS) (18, 20) at the luminal surface of ECs contribute to angiogenesis (36). ECs forming the inner lining of blood vessels are directly exposed to WSS, which plays a central key role in the growth and branching of capillary vessel networks (17). Capillary growth by sprouting of vessels increases with increasing levels of WSS (8). Sprouting angiogenesis is a common feature of venules, where stalk cells are generated leading to vessel outgrowth and capillary network formation (14). Post-capillary venules exposed to WSS in the range of 5 dyne/cm^2 are typically "hot spots" for angiogenic initiation (18, 23, 25); thus, the important question arises about the mechanism of sprouting angiogenesis at this relatively low level of ambient WSS. In addition, signals downstream that integrate biochemical and mechanical signals to control EC sprouting are defined poorly.

Membrane type 1-matrix metalloproteinase (MT1-MMP) regulates ECM remodeling and contributes to angiogenesis. Mice lacking MT1-MMP exhibited defective blood vessel invasion and fibroblast growth factor 2-induced corneal angiogenesis (44). MT1-MMP is also required for EC tubulogenesis and vascular lumen formation both in vitro and in vivo (6, 39). MT1-MMP is phosphorylated by S1P-induced Src activation to regulate membrane translocation and ECM proteolytic activity (28). Our recent studies have established a link between cytosolic Ca^{2+}-activated proteolytic enzymes and active MT1-MMP generation during angiogenesis (22, 27). Although these studies show that metalloproteinases such as MT1-MMP are required for angiogenesis, the intracellular molecular events that control MT1-MMP signaling in response to proangiogenic mediators and WSS in ECs are not defined.

Piezo1 is a Ca^{2+}-permeable transmembrane cation channel activated by physical force and consists of three pore-forming units that gate cations (13). Piezo1 is highly expressed in ECs (31, 35), where it directly senses the force imposed on endothelial cells by physiological shear stress in vascular development (31, 35). Global and endothelial cell-specific knockout of Piezo1 causes vascular defects and embryonic lethality (31, 35). Endothelial cell-specific Piezo1 knockout mice exhibited defective Ca^{2+} influx coupled to impaired EC alignment in response to WSS (31). Endothelial Piezo1 has been shown to be an important determinant of vascular architecture, but the role of Piezo1 in the process of angiogenesis remains incompletely understood. In this study, we used an in vitro WSS system, inducible EC-specific Piezo1-deficient mice, and multiple models of angiogenesis to demonstrate that Piezo1 was required for the angiogenesis response. Our results indicate that both WSS and S1P function by activating Piezo1 Ca^{2+} entry and metalloproteinases in ECs, which thereby signal angiogenesis.

* G. Hu and A. B. Malik contributed equally to this work and are co-senior authors.

Address for reprint requests and other correspondence: G. Hu, 3200W UICH, MC 515, Dept. of Anesthesiology, Univ. of Illinois College of Medicine, 1740 W. Taylor St., Chicago, IL 60612 (e-mail: gchu@uic.edu).

MATERIALS AND METHODS

Reagents. S1P (86492) was purchased from Avanti Polar Lipids. Anti-Piezo1 (SC164319), c-Src (SC-18 and SC-8056), and platelet/endothelial cell adhesion molecule-1 (PECAM-1 or CD31) (SC1505R) antibodies were obtained from Santa Cruz Biotechnology. Anti-Piezo1 (15939-1-AP), GAPDH (60004-1-lg), β-actin (60008-1-lg), and α-tubulin (66031-1-lg) antibodies were from Proteintech. Anti-phospho c-Src Tyr416 (2101) and PECAM-1 (3528) antibodies were purchased from Cell Signaling. Anti-MMP14 antibody (MAB3328) was obtained from EMD Millipore.

Mice. Piezo1 deletion in adult endothelia was achieved by tamoxifen administration to *Piezo1*$^{flox/flox}$ mice (C57BL/6J background; a kind gift from Dr. David J. Beech, University of Leeds, Leeds, UK) (31) crossed with stem cell leukemia (SCL)-Cre-ER^{T} mice. We used the 5′-endothelial enhancer of SCL-Cre, which is not expressed in adult mouse bone marrow or adult mouse hematopoietic lineage cells (15), to ensure that deletion of Piezo1 was restricted to endothelial lineage cells in the adult mice. Littermates (*Piezo1*$^{flox/flox}$) that were null for the Cre gene were used as controls. Piezo1 deletion in adult 4-wk-old mice was induced by tamoxifen administration (2 mg/day ip for 5 days). Age- and sex-matched wild-type mice were used in identical tamoxifen regimen to control for any nonspecific effects of tamoxifen on the endothelium. All animal procedures were approved by the Animal Care and Use Committee of the University of Illinois at Chicago.

For genotyping, DNA from each tail (4–6 mm) was extracted using the DNEasy tail extraction kit (Qiagen cat. no. 69504). Each tail sample was placed in a 1.5-ml microcentrifuge tube and ground under 180 μl of Buffer ATL before addition of 20 μl of proteinase K and incubation at 56°C for 1 h. Samples were periodically vortexed during digestion before addition of 200 μl of Buffer AL and 200 μl of ethanol, and vortexing again. DNA was purified by centrifuging in a DNEasy Mini spin column with two purification buffers (AW1 and AW2) and then eluted in 150 μl of Buffer AE at 56°C for 5 min. Genotyping primers are listed in Table 1. PCR conditions were as follows: 95°C for 5 min, 30 cycles of 95°C for 30 s, 63°C for 30 s, and 72°C for 20 s, and then 72°C for 5 min. Successful Cre-driven deletion was confirmed by PCR.

Cell culture. Human umbilical vein endothelial cells (HUVECs) were cultured in T-75 flasks on 0.1% gelatin in EGM-2 medium (endothelial basal medium-2 supplemented with bullet kit additives plus 10% FBS) at 37°C in a humidified incubator with 5% CO_2.

Isolation of mouse lung endothelial cells. Isolation of lung ECs was performed as reported, with minor modifications (12). Briefly, the lung was soaked in perfusion PBS medium and then removed. To facilitate digestion, lungs were placed with PBS into a 10-cm culture dish and minced into 1-mm^3 pieces and processed by enzymatic digestion: 1 mg/ml collagenase (Sigma, St. Louis, MO). The suspension was incubated at 37°C on a rotary shaker for 30 min. The suspension was triturated using a 21-gauge needle and filtered through a 70-μm nylon mesh filter prior to washing in PBS buffer containing 0.5% BSA in the absence of Ca^{2+}. The suspension was centrifuged at 300 *g* for 5 min, and the supernatant was aspirated out. Cells were treated with red blood cell lysis buffer and centrifuged at 14,000 *g* for 10 min. The cell suspension was incubated with PECAM-1 antibody for 30 min before adding CD31 microbeads at 4°C for 30 min. CD31 microbeads were separated in a tube magnet, and the suspension buffer contained non-ECs. Cells were used at passages 3–5. ECs were characterized by their cobblestone morphology and PECAM-1 expression.

Table 1. *Primer sequences for PCR analysis*

Gene	PCR Primer (5′–3′)
LoxP-spanning (155, 189 bp)	F: GGAGGGTTGCTTGTTGGATA
	R: ACTCATCTGGGTGAGGTTGC
SCL-Cre (482 bp)	F: TCGATGCAACGAGTGATGAG
	R: TTCGGCTATACGTAACAGGG
Cre deletion-spanning (379 bp)	F: ACCACCTGAGAAGTTGTCCC
	R: ACTCATCTGGGTGAGGTTGC

F, forward; R, reverse.

Table 2. *Nontargeting and Piezo1 siRNA sequences*

Gene	siRNA Sequence (5′–3′)
Nontargeting	UGGUUUACAUGUCGACUAA
	UGGUUUACAUGUUGUGUGA
	UGGUUUACAUGUUUUCUGA
	UGGUUUACAUGUUUUCCUA
Piezo1 (P1-1 si)	SMARTpool (L-020870-03-0005, Dharmacon)
Piezo1 (P1-2 si)	UGGAGUAUGCCAACGAGAA
	GCAGCAUGACAGACGACAU
	GCGCAUCAGUCUACGUUUU

Cell transfection. Endothelial cells cultured in a 25-cm^2 flask were transfected with 100 nM small interfering (si)RNAs in opti-MEM using Oligofectamine. At 4 h after transfection, cells were supplemented with 3 ml of opti-MEM including 20% fetal bovine serum (FBS). After 24 h, the flasks were aspirated and supplemented with fresh EGM-2 medium. These ECs were transferred to the WSS system, where they formed a monolayer as described above. Protein expression in siRNA-treated ECs was assessed by Western blotting. The sequences of control and Piezo1 siRNAs are listed in Table 2.

To assess localization of MT1-MMP, plasmids expressing MT1-MMP DNA (6 μg) fused to red (RFP) or green fluorescent protein (GFP) were diluted in 500 μl of Opti-MEM for 5 min and then mixed with Lipofectamine 2000 for 20 min. ECs were trypsinized, pelleted, and resuspended in 3 ml of endothelial basal medium-2 (EBM2) with 20% FBS. Cell suspensions (1 ml) were incubated with the DNA/Lipofectamine complexes and seeded onto glass slides for 2 h before addition of EGM-2 without antibiotics.

Endothelial cell wound healing assay. Endothelial monolayers in plates were transfected with control or Piezo1 siRNA. At 48 h posttransfection, the monolayers were wounded gently using a single pass with a sterile pipette tip and washed twice in sterile PBS, and the medium was replaced with supplemented EBM2 medium containing reduced serum supplement II (RSII) and ascorbic acid (AA) in the presence of S1P. At 18 h after injury, the cultures were washed in PBS, fixed in 3% glutaraldehyde solution in PBS for 2 h, and stained with 0.1% toluidine blue in 30% methanol for 15 min. Images were obtained with a microscope equipped with a digital camera. The area covered by the cells was measured using ImageJ (NIH, Bethesda, MD).

Analysis of cell viability. Lactate dehydrogenase (LDH) activity, a marker for cell death, was measured with a LDH detection kit (Roche Diagnostics, Indianapolis, IN) according to the manufacturer's instructions. LDH activity was detected by at 450 nm with a 96-well plate reader and expressed as a percentage of LDH in medium to total LDH.

Plasmids and viral constructs. MT1-MMP-GFP were created using PCR primers designed to amplify from human cDNA the full-length MT1-MMP gene (GenBank accession no. NM_004995). The PCR product was digested and ligated to AviGFPc1 vector via 5′-*EcoRI* and 3′-*KpnI*. MT1-MMP-RFP were created from MT1-MMP-GFP.

Measurement of cell surface MT1-MMP expression. Endothelial cell monolayers were serum starved for 2 h, incubated in the WSS system in the presence of S1P for 2 h, fixed, and then imaged. To quantify the cell surface expression of MT1-MMP-RFP or -GFP, thresholding was used to create a binary image. The noise was then lowered using a "despeckle" filter. Any perinuclear staining that entered the outline was excluded from our analysis. The integrated intensity was employed as the extent of MT1-MMP localization to the cell periphery. Fluorescent images were captured on a Zeiss LSM710 or LSM880 confocal microscope (Carl Zeiss, Goettingen, Germany) using a ×40 or ×63 objective.

Western blotting. Endothelial cells were washed with cold Hanks' balanced salt solution (ThermoFisher, no. 14175), lysed in cold RIPA

buffer (ThermoFisher, no. 89900) containing phenylmethylsulfonyl fluoride, sodium vanadate, and protease and phosphatase inhibitor cocktail for 10 min at 4°C under rotation, centrifuged at 14,000 *g* for 10 min, and frozen at −80°C. To denature, samples were mixed with Laemmli sample buffer (Bio-Rad, no. 161-0747) and then boiled at 95–100°C for 5 min. Proteins were separated by electrophoresis on a 6–10% SDS polyacrylamide gel and transferred to nitrocellulose membranes. After blocking in 5% milk or BSA at room temperature for 1 h, the membranes were incubated with primary antibody at 4°C overnight in Tris-Tween 20 saline. Membranes were washed three times in Tris-Tween 20 saline before incubation with secondary antibody in Tris-Tween 20 saline containing 5% milk for 1 h. Band intensities were measured using ImageJ software.

Wall shear stress system. The WSS system was established as described previously (20). Briefly, a silicone rubber membrane containing perforated holes was adhered to glass microscope slides to form circular wells. Collagen matrix (rat tail collagen type I, 7.1 mg/ml) (20) was prepared and allowed to polymerize onto the membrane for 30 min at 37°C in a humidified 5% CO_2 incubator. Endothelial cells were then seeded onto the collagen matrix, where they formed a confluent monolayer. The perfusion medium consisted of EBM2 containing reduced serum supplement II (RSII) at 1:250 dilution and 50 μg/ml ascorbic acid (22). The plates containing the EC monolayer on the collagen matrix were assembled into a parallel plate flow chamber designed to apply uniform WSS to the EC monolayer. WSS magnitude was calculated using the equation: $\tau = 6\ \mu Q/wh^2$, where τ is wall shear stress, μ is fluid viscosity (0.7 centipoise), Q is flow, w is width of the channel (29.2 mm), and h is height of flow channel. The ECs in the WSS system were allowed to invade the matrix for 24 h. In some experiments, S1P was added during the collagen polymerization step.

Treatment with Piezo1 inhibitor GsMTx4 and activator Yoda1. Endothelial cells were preincubated with the spider peptide grammostola spatulata mechanotoxin 4 (GsMTx4, Tocris Bioscience) (1, 31, 34) for 1 h before applying the WSS. In other studies, ECs were seeded on the collagen matrix including S1P for 18 h in the presence of either vehicle or 1 μM Yoda1 (2-[5-[[(2,6-dichlorophenyl) methyl]thio]-1,3,4-thiadiazol-2-yl]-pyrazine) (2, 40).

Measurement of vessel sprouting in three-dimensional-collagen matrix. To quantify EC invasion in a three-dimensional (3D) collagen gel of the WSS system, the collagen matrix containing invading cells was washed briefly in PBS, fixed in 3% glutaraldehyde solution in PBS for 2 h, stained with 0.1% toluidine blue in 30% methanol for 15 min, and washed with water to identify invading ECs, as described (21). The number, thickness, and length of vessel sprouts were quantified. Cross-sectional digital images were collected using an Olympus BX51/IX70 fluorescence microscope with a camera.

RapR-Src activation. RapR-Src and mCherry FRB retroviral constructs were generated as described (5). ECs were infected with RapR-Src and FRB viral supernatants for 24 h and stimulated with 0.5 μM rapamycin to activate Src for 1 h.

Intracellular Ca^{2+} measurement. Endothelial cells were grown to confluence on clear-bottom 96-well plates. Before recording, cells were loaded with a FLIPR-5 Ca^{2+}-sensitive fluorescence indicator (Molecular Devices, Sunnyvale, CA) for 30 min at 37°C. Addition of test reagents was robotically controlled, and monolayer fluorescence in each well was read by Flexstation data acquisition system (Molecular Devices) at 0.1 Hz.

Zymography. Conditioned medium was obtained from the WSS system reservoir and centrifuged at 500 *g* for 5 min, and the supernatants were collected and frozen at −80°C. Aliquots of conditioned medium were concentrated ~10-fold using a Centricon centrifugal filter unit containing an Ultracel YM-10 membrane (Millipore) at 5,000 rpm at 4°C. The concentrated media prepared under nonreducing conditions were loaded into 8.5% acrylamide gels containing a final concentration of 1 mg/ml porcine gelatin. Following electrophoresis, the matrix was rinsed three times in 100 ml of 2% Triton X-100 for 1 h and twice in distilled water before being placed in 25 mM Tris·HCl (pH 7.5) containing 5 mM $CaCl_2$ overnight. The gels were stained with 0.1% Coomassie blue in 30% methanol and 10% acetic acid for 20 min at room temperature and destained in 30% methanol and 10% acetic acid before image analysis.

Matrigel plug assay in mice. Piezo1$^{flox/flox}$ (*P1$^{fl/fl}$*) and EC-specific deletion of Piezo1 (*P1$^{iEC\text{-}KO}$*) mice were injected subcutaneously in the midventral abdominal region with 250 μl of the growth factor reduced Matrigel (BD Biosciences) at a final concentration of 9 mg/ml, containing S1P (2 μM) and VEGF (100 ng/ml). Samples from the Matrigel plugs were isolated after 14 days of implantation, fixed in 4% paraformaldehyde, dehydrated in alcohol, cleared in xylene, and embedded in paraffin. Sections (5 μm) of the plugs were stained with hematoxylin and eosin (H&E). For immunohistochemistry, tissue sections were deparaffinized in xylene and rehydrated with decreasing concentrations of alcohol. Endogenous peroxide was blocked with hydrogen peroxide, and antigen retrieval was carried out by 10 mM citrate buffer (with 0.05% Tween 20 at pH 6.0) for 30 min in a pressure cooker. After blocking in 10% donkey serum in PBS, tissue sections were stained with primary antibodies anti-*Bandeiraea simplicifolia* isolectin B4 or biotin conjugate antibody (BSI-B4, 1:200; Sigma, L2140). Streptavidin-peroxidase was used as a secondary antibody.

Aortic ring capillary sprouting assay. Thoracic aorta was freshly harvested from mice and cleaned, and then 1-mm segments were placed in 100 μl of cold rat tail collagen type I supplemented with S1P (1 μM) and VEGF (100 ng/ml) in a 96-well plate for 4 days. After 30 min in a 37°C incubator, EGM-2 was changed every other day. Capillary sprouting was counted by phase-contrast microscopy with the use of at least six segments of aorta per group. Aortic ring sprouts were analyzed through morphological differences in growth between the endothelial sprouts and fibroblast sprouts based on greater thickness and a uniform pattern of growth of endothelial sprouts. Aortic sprout length was calculated with AxioVision LE software.

Mouse hindlimb ischemia model. Following anesthesia (87 mg/kg ketamine + 13 mg/kg xylazine), the left femoral artery was exposed under a dissection microscope. The proximal portion of the femoral artery and the distal portion of the saphenous artery were ligated. All branches between these two sites were ligated or cauterized, and an arteriotomy was performed. The ischemic (left)-to-nonischemic (right) limb blood flow ratio was measured using a laser Doppler blood flow analyzer (PeriScan PIM 3 System, Perimed) as described (37). Mice were placed on a heating plate at 37°C for 10 min to minimize temperature variation. Before and after surgery, laser Doppler blood flow (LDBF) analysis was performed in the plantar sole. Blood flow was displaced as changes in the laser frequency, represented by different color pixels. Mean LDBF values were expressed as the ratio of ischemic to nonischmic LDBF.

Wound closure assay in mice. Wound closure rates were studied in *P1$^{fl/fl}$* and *P1$^{iEC\text{-}KO}$* mice as described previously (33). The dorsum area was clipped and treated with a depilatory cream (Nair) to remove remaining hair. Skin was prepared with Betadine and allowed to dry. Wounds were dressed with a bioclusive transparent oxygen-permeable wound dressing (Johnson & Johnson). Digital images of wounds were taken, and wound diameters were measured using ImageJ software.

Statistical analysis. Data are presented as mean ± SE for each group of samples. Statistical analysis was performed with GraphPad Prism 5.0. Comparisons between two groups were performed using two-tailed unpaired Student *t*-tests. Comparisons between three or more groups were performed by one-way ANOVA with post hoc Tukey test. Differences were considered significant when $P < 0.05$.

RESULTS

Piezo1 is required for sprouting angiogenesis. To address the role of Piezo1 in regulating angiogenesis, we used the parallel-plate flow WSS system, in which varying amounts of

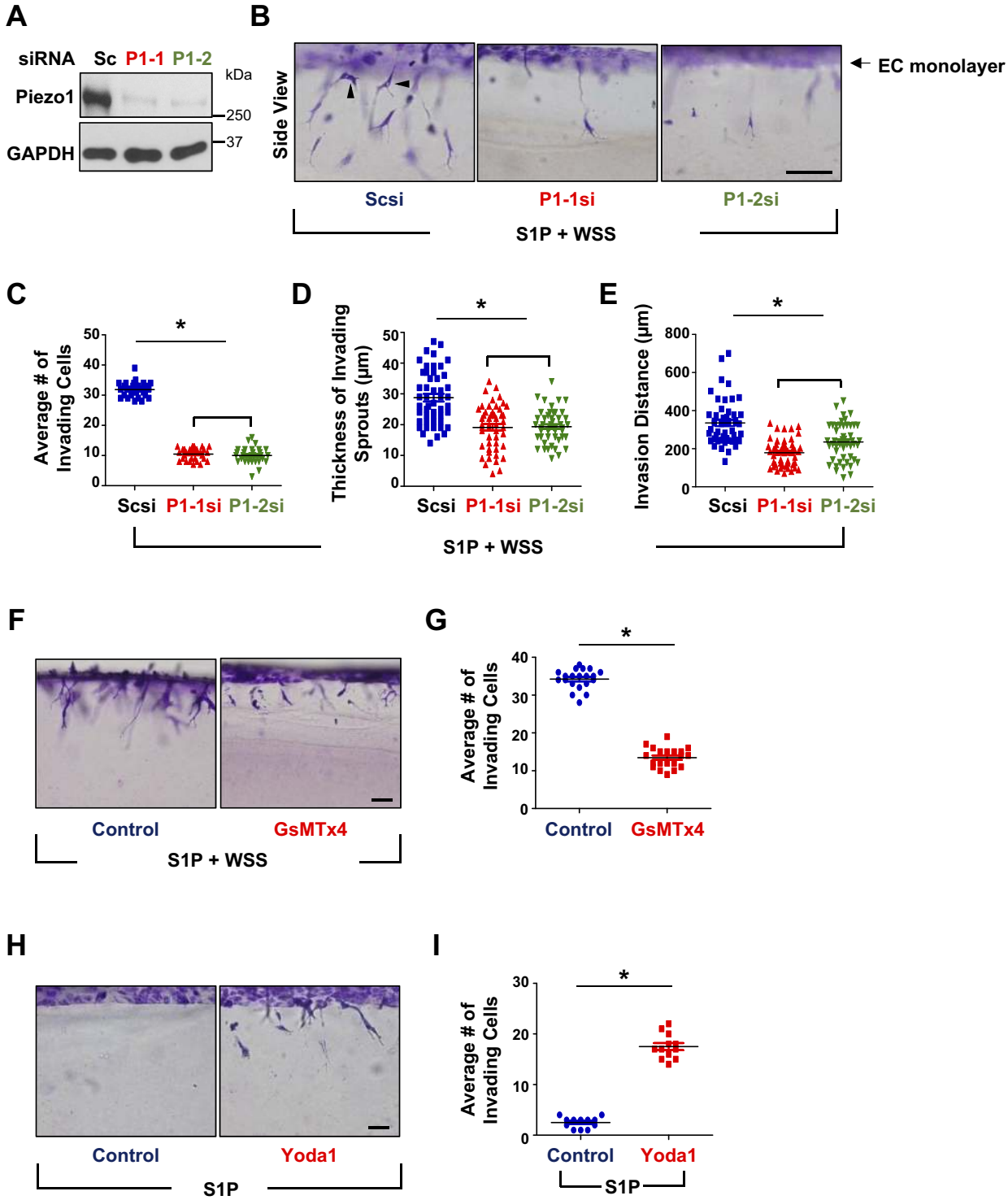

Fig. 1. Piezo1 is required for sprouting angiogenesis. *A*: immunoblotting showing depletion of Piezo1 by two different siRNAs employed [Piezo1 KD1 (P1-1si) and Piezo1 KD2 (P1-2si)]. Scrambled siRNA (Scsi) serves as a control. Each blot is representative of 3 independent experiments. *B*: representative micrographs showing that augmented angiogenesis in response to wall shear stress (WSS) plus sphingosine 1-phosphate (S1P) is prevented by depleting Piezo1. Arrowheads show lumen formation. Scale bar, 200 μm. *C–E*: depletion of Piezo1 prevented endothelial cell (EC) sprouting. ECs transfected with Scsi or P1-1si were subjected to 5 dyne/cm^2 WSS on a 3D collagen matrix. Quantification of the number of invading ECs (*C*), thickness of invading sprouts (*D*), and EC invasion distance (*E*). Four independent experiments were performed. Total of 30 wells (monolayers) were counted; $n = 50$ sprouts. *$P < 0.05$, 1-way ANOVA. *F* and *G*: grammostola spatulata mechanotoxin 4 (GsMTx4) prevents EC invasion. *F*: representative cross-sectional micrographs are shown. ECs were preincubated with GsMTX4 for 1 h prior and then subjected to S1P (1 μM) plus WSS (5 dyne/cm^2) for 18 h. Scale bar, 200 μm. *G*: quantification of EC invasion density. Three independent experiments were performed; $n = 20$ wells. *$P < 0.05$, Student's *t*-test. *H* and *I*: Yoda1 (2-[5-[[(2,6-dichlorophenyl)methyl]thio]-1,3,4-thiadiazol-2-yl]-pyrazine) enhanced EC invasion. *H*: representative cross-sectional micrographs are shown. EC monolayer on collagen matrix was subjected to S1P (1 μM) for 18 h in the presence of vehicle or Yoda1 (1 μM). Scale bar, 200 μm. *I*: quantification of EC invasion density. Three independent experiments were performed; $n = 12$ wells. *$P < 0.05$, Student's *t*-test.

WSS can be applied (20), and S1P was added to the collagen matrices at physiological concentration of 1 μM. This system enabled quantification of sprouting angiogenesis into the 3D collagen matrix, as described by us (20). The WSS level of 5 dyne/cm^2 was chosen as it is typical in venules (18, 25, 26). We observed successful depletion of Piezo1 by either of the two specific siRNAs used (Fig. 1*A*). Piezo1 depletion prevented lumen formation in sprouting vessels following WSS and S1P stimulation compared with control group (Fig. 1*B*). Depletion of Piezo2 failed to prevent angiogenesis (data not shown). Piezo1 depletion also significantly reduced the number of invading ECs (Fig. 1*C*), thickness of sprouts (Fig. 1*D*), and invasion distance of sprouts (Fig. 1*E*) compared with control siRNA. Consistently, the pharmacological Piezo1 channel inhibitor GsMTx4 (1, 31, 34) markedly reduced vessel sprouting (Fig. 1, *F* and *G*), whereas the selective Piezo1 activator Yoda1 (2, 40) was able to induce sprouting angiogenesis (Fig. 1, *H* and *I*). GsMTx4 did not alter EC viability even at the dose of 20 μm (data not shown). These results clearly demonstrate that Piezo1 is required for EC sprouting angiogenesis into the 3D collagen matrix in response to S1P/WSS stimulation.

S1P activation of Piezo1 mediates Ca^{2+} entry in endothelial cells and capillary network formation. Piezo1 is known as an ion channel that senses a wide range of mechanical stimuli (2, 10). We next examined whether S1P also influences the Piezo1-activated Ca^{2+} entry in ECs. Interestingly, we found that depletion of Piezo1 by siRNAs dramatically reduced Ca^{2+} entry and peak height and delayed the rise and recovery rates of the Ca^{2+} changes in ECs in response to S1P stimulation (Fig. 2, *A* and *B*), suggesting that S1P regulates the Piezo1 Ca^{2+} gating function. The pharmacological Piezo1 inhibitor GsMTx4 also significantly diminished Ca^{2+} entry following

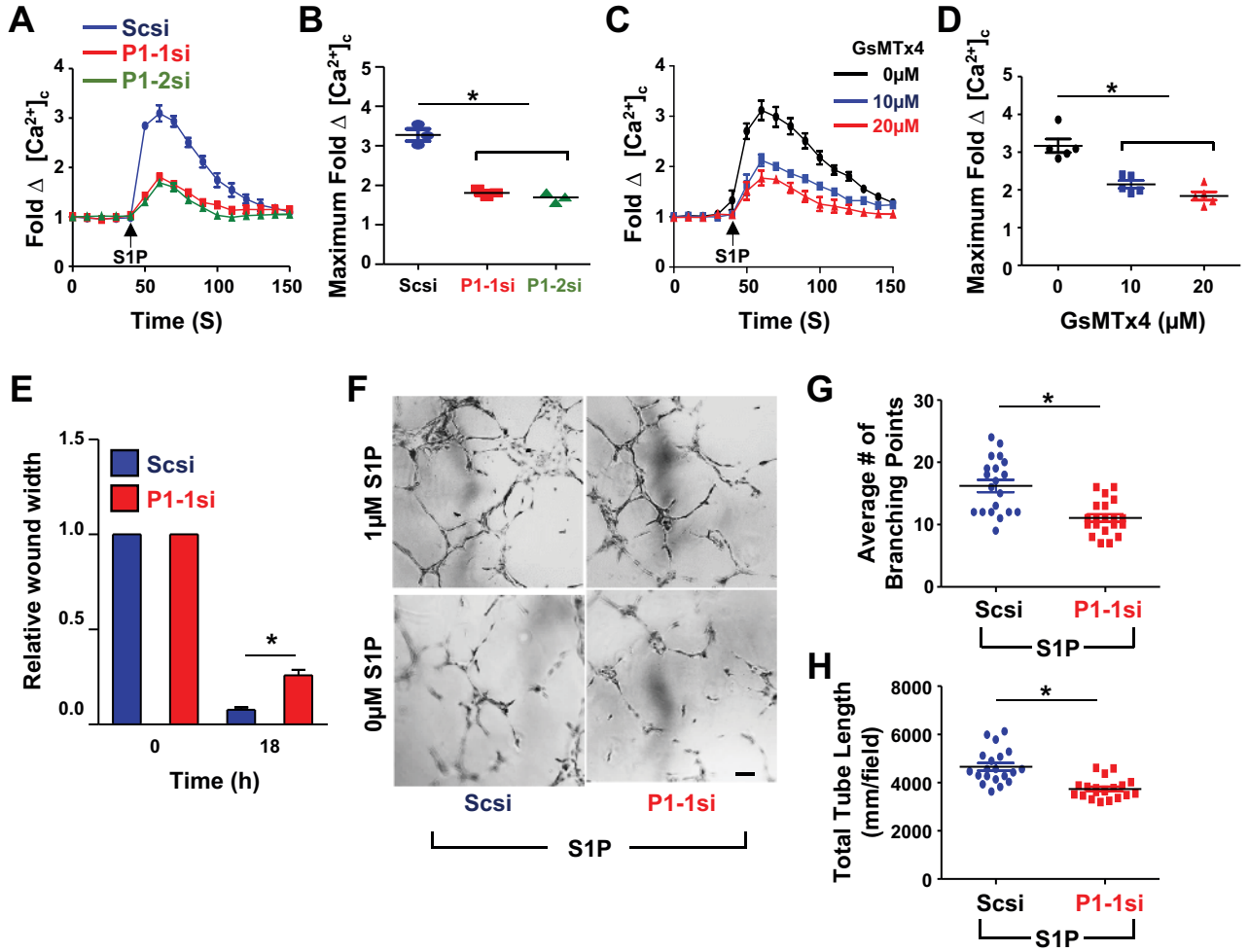

Fig. 2. Piezo1 induces sphingosine 1-phosphate (S1P)-dependent Ca^{2+} entry in endothelial cells (ECs) and capillary formation. *A* and *B*: depletion of Piezo1 reduced S1P-induced Ca^{2+} entry in EC monolayers. Piezo1 was depleted by two different siRNAs employed (Piezo1 KD1 (P1-1si) and Piezo1 KD2 (P1-2si)). Scrambled siRNA (Scsi) serves as a control. *A*: representative tracing is shown. *B*: mean of maximum responses is expressed in scattered dot plot. Data were from 3 independent experiments, each performed in triplicate; $n = 9$ replicates. *$P < 0.05$, 1-way ANOVA. *C* and *D*: treatment of ECs with grammostola spatulata mechanotoxin 4 (GsMTx4) reduced S1P-induced Ca^{2+} entry. *C*: representative tracing is shown. *D*: mean of maximum responses is expressed in scattered dot plot. Data were from 3 independent experiments each performed in triplicate; $n = 9$ replicates. *$P < 0.05$, 1-way ANOVA. *E*: Piezo1 depletion induces defective S1P-induced EC migration in the wound healing assay. ECs transfected with Piezo1 KD1 or scrambled siRNA were subjected to the same wound scratch healing assay in the presence of S1P for 18 h. Data were from 3 independent experiments each performed in triplicate; $n = 8$ wound areas. *$P < 0.05$, Student's *t*-test. *F–H*: Piezo1 depletion impaired S1P-induced capillary network formation. ECs transfected with Piezo1 KD1 (P1-1si), or Scsi were seeded in Matrigel in the presence of S1P for 14 h. *F*: representative capillary network formation was shown. Number of branch points (*G*) and tube length (*H*) was calculated. Scale bar, 100 μm. Three independent experiments were performed; $n = 12$ wells. *$P < 0.05$, Student's *t*-test.

S1P addition in ECs in a concentration-dependent manner (Fig. 2, *C* and *D*), further supporting the role of S1P in regulating Piezo1 channel function. We also observed that Piezo1 depletion by specific siRNAs resulted in a severe reduction in EC migration (Fig. 2*E*), capillary network formation (Fig. 2*F*), number of vessel branch points (Fig. 2*G*), and length of tubes formed (Fig. 2*H*) in response to S1P treatment. Taken together, our results suggest the important role of S1P activation of Piezo1 in the mechanism of angiogenesis.

Src activation stimulates Piezo1 Ca^{2+} gating to signal sprouting angiogenesis. We sought to elucidate the molecular mechanism by which proangiogenic factor S1P stimulates Piezo1-mediated Ca^{2+} signaling. Western blot analysis indicated that S1P at the concentration of 1 μM increased Src phosphorylation at Tyr416 (activation) compared with control ECs (Fig. 3, *A* and *B*), consistent with the previous findings (41). Next, we addressed whether Src activation was able to activate Piezo1-mediated Ca^{2+} influx. We observed that depletion of Src markedly reduced S1P-induced Ca^{2+} influx (Fig. 3, *C* and *D*). Using the RapR-Src system (Fig. 3*E*) to activate c-Src in ECs (45), we found that activation of Src increased Ca^{2+} influx, whereas depletion of Piezo1 by a specific siRNA prevented this response (Figs. 3, *F* and *G*), suggesting that c-Src lies upstream of the Ca^{2+} gating function of Piezo1 in response to S1P stimulation. Thus, Src-mediated Piezo1 Ca^{2+} gating may contribute to the role of S1P in sprouting angiogenesis.

Piezo1 mediates sprouting angiogenesis through metalloproteinase activation. Activation of metalloproteinases in ECs has been shown to be essential for sprouting angiogenesis (6, 22, 27, 39). As expected, gelatin zymography showed that exposure of ECs to WSS/S1P increased promatrix metalloproteinase-2 (pro-MMP2) expression and proteolytically processed the MMP2 proenzyme to its active 67-kDa forms in a time-dependent manner, and these responses were prevented by Piezo1 depletion (Fig. 4, *A–C*). Because Pro-MMP2 is activated on the cell surface by MT1-MMP (22, 24), we thus examined whether Piezo1 could regulate MT1-MMP activity. Surprisingly, Piezo1 depletion only slightly reduced MT1-MMP activation in 3D collagen matrix (Fig. 4*D*). It seems that reduced levels of MT1-MMP activation by Piezo1 siRNA did

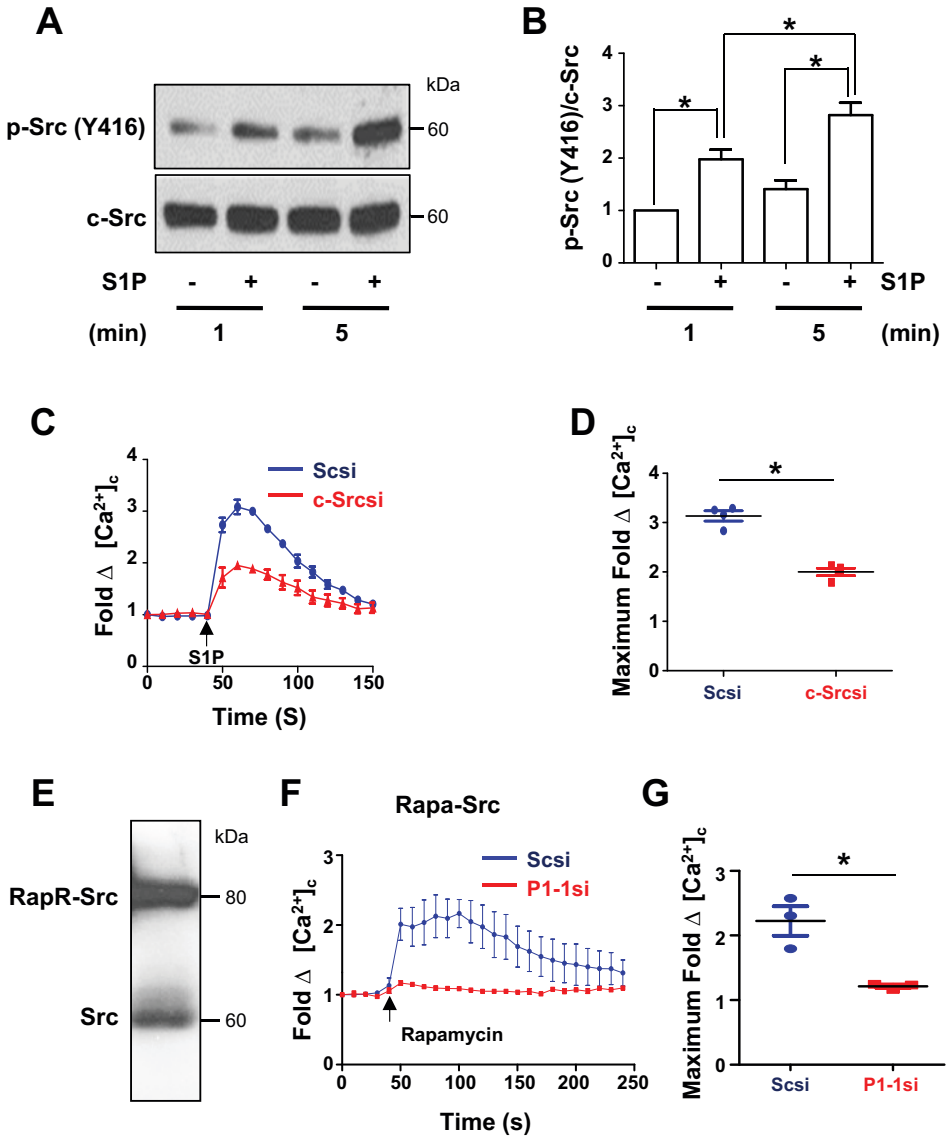

Fig. 3. Src activation stimulates Piezo1 Ca^{2+} gating following sphingosine 1-phosphate (S1P) stimulation. *A* and *B*: S1P increased Src phosphorylation at Tyr416 (Y416). Endothelial cells (ECs) were serum starved for 2 h and then treated with or without S1P for 1 or 5 min. Cell lysates were immunoblotted with anti-phospho-Src (Y416) or anti-c-Src antibodies. *A*: representative Western blots for phospho-Src and c-Src. *B*: protein quantification by densitometry. Data were from 3 independent experiments. *$P < 0.05$, 1-way ANOVA. *C* and *D*: Src knockdown reduced Ca^{2+} entry in response to S1P stimulation. ECs were transfected with scrambled (Scsi) or c-Src siRNA (cSrcsi). At 48 h posttransfection, ECs were serum starved for 2 h and then then treated with or without S1P for the indicated time. *C*: representative tracing is shown. *D*: mean of maximum responses is expressed in scattered dot plot. Data were from 4 independent experiments, each performed in triplicate.*$P < 0.05$, Student *t* test. *E*: exogenous expression of RapR-Src. ECs were infected with adenovirus expressing RapR-Src-cerulean-myc for 24 h. Cell lysates were collected for immunoblotting. *F* and *G*: constitutive Src activation by exogenous expression of the RapR-Src construct induced Ca^{2+} entry via Piezo1. ECs treated with control or Piezo1 siRNA were transfected with mCherry-FRB and RapR-Src overnight. Before recording, cells were loaded with FLIPR-5 Ca^{2+}-sensitive fluorescence indicator for 30 min at 37°C. Addition of rapamycin (0.5 μM) was robotically controlled, and monolayer fluoresce in each well was read by Flexstation data acquisition system. *F*: representative tracing is shown. *G*: mean of maximum responses is expressed in scattered dot plot. Data were from 3 independent experiments, each performed in triplicate. *$P < 0.05$, Student's *t*-test.

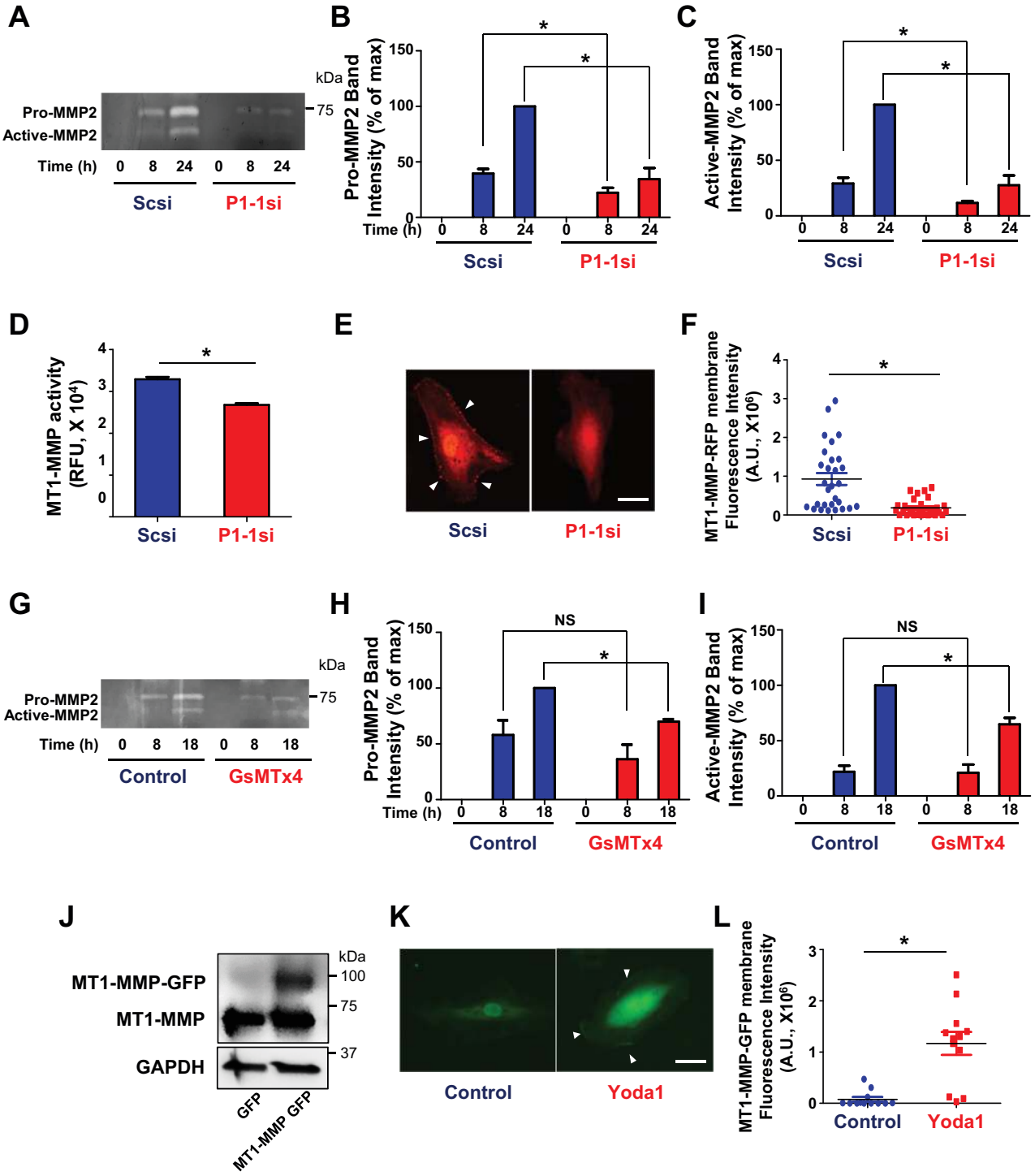

Fig. 4. Piezo1 mediates metalloproteinase activation. *A–C*: Piezo1 depletion reduced the release of matrix metalloproteinase-2 (MMP2). Conditioned medium was collected for gelatin zymography at indicated time points. Concentrations of MMP2 propeptide (Pro-MMP2) and Active-MMP2 are shown by gelatin zymography (*A*) and quantified by densitometric analysis (*B* and *C*). Band intensities were normalized relative to highest intensity for Pro- or Active-MMP2. Data were from 3 independent experiments. *$P < 0.05$, 1-way ANOVA. *D*: Piezo1 depletion reduced membrane type 1 (MT1)-MMP activation. Data were from 3 independent experiments, each performed in triplicate. *$P < 0.05$, Student's *t*-test. *E* and *F*: Piezo1 depletion prevented MT1-MMP membrane translocation. ECs transiently transfected with vectors expressing MT1-MMP-RFP constructs were treated with sphingosine 1-phosphate (S1P) and wall shear stress (WSS). *E*: representative micrographs are shown. Scale bar, 10 μm. *F*: MT1-MMP RFP membrane fluorescence intensities were quantified. Data were from 3 independent experiments; $n = 30$ cells. *$P < 0.05$, Student's *t*-test. *G–I*: grammostola spatulata mechanotoxin 4 (GsMTx4) suppressed the release of Pro- and Active-MMP2. Conditioned medium was collected for gelatin zymography (*G*) at indicated time points for measurement of pro-MMP2 activity (*H*) and Active-MMP2 (*I*). Data were from 3 independent experiments. *$P < 0.05$, 1-way ANOVA. *J–L*: activation of Piezo1 by Yoda1 (2-[5-[[(2,6-dichlorophenyl)methyl]thio]-1,3,4-thiadiazol-2-yl]-pyrazine) enhanced MT1-MMP membrane localization. ECs transiently transfected with vectors expressing MT1-MMP-GFP constructs (*J*) were serum starved for 2 h followed by stimulation with or without Yoda1 (1 μM) for 2 h. *K*: representative micrographs are shown. Arrowheads show MT1-MMP-GFP localized in EC periphery indicative of MT1-MMP activation. Scale bar, 10 μm. *L*: MT1-MMP green fluorescent protein (GFP) membrane fluorescence intensities from *K*. Data were from 3 independent experiments; $n = 12$ cells. *$P < 0.05$, Student's *t*-test.

not completely explain the role of Piezo1 in regulating invasion responses elicited by S1P plus 5 dyne/cm^2 WSS. On the basis of our previous finding that increased MT1-MMP plasma membrane translocation correlated with increased EC sprouting responses (21, 22), we determined the role of Piezo1 in the translocation of MT1-MMP-RFP to the EC plasma membrane and found that Piezo1 depletion almost completely inhibited MT1-MMP-RFP membrane translocation (Fig. 4, *E* and *F*). Furthermore, gelatin zymography showed that the Piezo1 channel inhibitor GsMTx4 suppressed the release of pro- and active MMP2 (Fig. 4, *G–I*), whereas the specific activator of Piezo1, Yoda1, induced exogenous MT1-MMP-GFP (Fig. 4*J*) membrane translocation (Fig. 4, *K* and *L*), confirming the above results. These data suggest that Piezo1 promotes angiogenesis following WSS/S1P stimulation through modulating the MT1-MMP/MMP2 signaling pathway.

Angiogenesis was markedly inhibited in endothelial cell-specific Piezo 1-deficient mice. To study the functional significance of Piezo1 expression in endothelial cells in angiogenesis, we generated EC-specific deletion of Piezo1 mice [$P1^{iEC\text{-}KO}$ mice; *Piezo1*$^{flox/flox}$ ($P1^{fl/fl}$) × *SCL-Cre*). SCL-Cre and Piezo1-flox alleles in mice were identified by PCR (Fig. 5*A*). We engineered mice with conditional Cre-Lox-mediated disruption of Piezo1 (Fig. 5*B*). Specificity and efficiency of Piezo1 deletion in endothelial cells were confirmed by PCR and Western blotting (Fig. 5, *C* and *D*). We found an ~95% reduction in Piezo1 protein levels in isolated mouse lung endothelial cells but not in non-endothelial cells (epithelial cells and fibroblasts; Fig. 5*D*). These data demonstrate that tamoxifen treatment induced endothelial cells-restricted deletion of Piezo1. There were no significant differences between genotypes in home cage activity, reproductive phenotype, body weight, and vascular phenotype.

We next assessed the role of Piezo1 in mediating angiogenesis in $P1^{iEC\text{-}KO}$ mice with the response compared with control $P1^{fl/fl}$ mice. $P1^{fl/fl}$ and $P1^{iEC\text{-}KO}$ mice were both injected subcutaneously with Matrigel plugs supplemented with S1P (2 μM) in the midventral abdominal region. We observed that administration of S1P induced vessel formation in the plugs obtained from $P1^{fl/fl}$ mice (Fig. 6*A*), whereas the plugs from $P1^{iEC\text{-}KO}$ mice showed a markedly reduced level of BSI-B4, the lectin that marks vessel formation (Fig. 6*B*) and angiogenic area (Fig. 6*C*). The mouse aortic ring assay showed impaired capillary sprouting and reduced sprouting area in aortic rings exposed to S1P from $P1^{iEC\text{-}KO}$ mice compared with those from $P1^{fl/fl}$ mice (Fig. 6, *D* and *E*). We also determined the role of

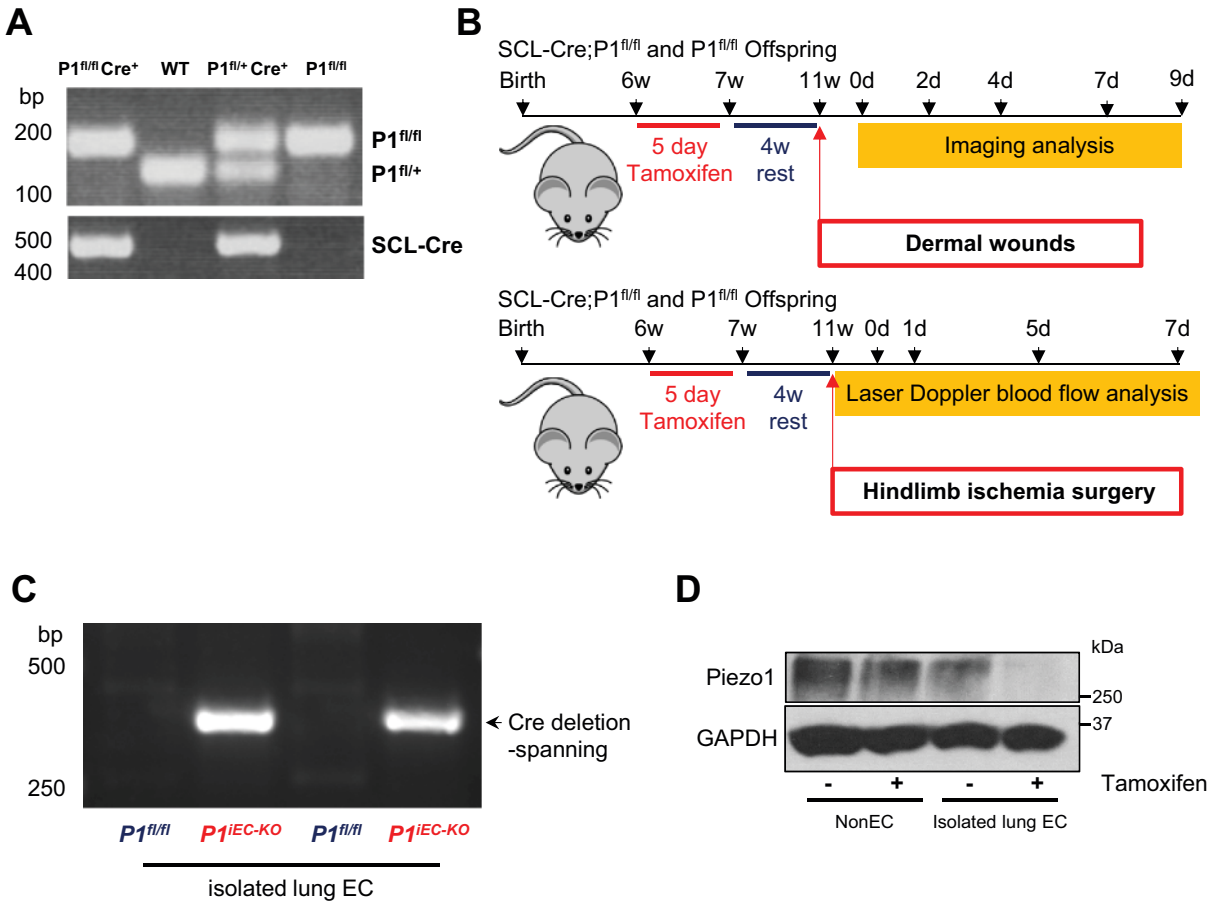

Fig. 5. Characterization of endothelium-specific Piezo1 knockout ($P1^{iEC\text{-}KO}$) mice. *A*: PCR genotyping assay used for tailsnip genomic DNA from a Piezo1$^{flox/flox}$ ($P1^{fl/fl}$) and SCL-Cre$^+$ (*lane 1*), wild type (WT; *lane 2*), Piezo1$^{flox/+}$ and SCL-Cre$^+$ (*lane 3*), and $P1^{fl/fl}$ mice (*lane 4*) *B*: Experimental protocols for the induction of endothelial Piezo1 ablation in mice. *C*: example genotyping results with loxP-spanning PCR primers. A specific 379-bp band indicated deletion. Product was detected in two $P1^{iEC\text{-}KO}$ mice. Mice with the 379-bp band were labeled *iEC-KO* to indicate disruptive deletion in Piezo1 of endothelial cells (ECs). Mice labeled as $P1^{fl/fl}$ mice showed no 379-bp band. *D*: effects of tamoxifen treatment of SCL-Cre-ER^T;$P1^{fl/fl}$ mice on Piezo1 protein levels in non-ECs and ECs. Cells were isolated, and lysates were analyzed by immunoblotting using Piezo1 or GAPDH antibodies.

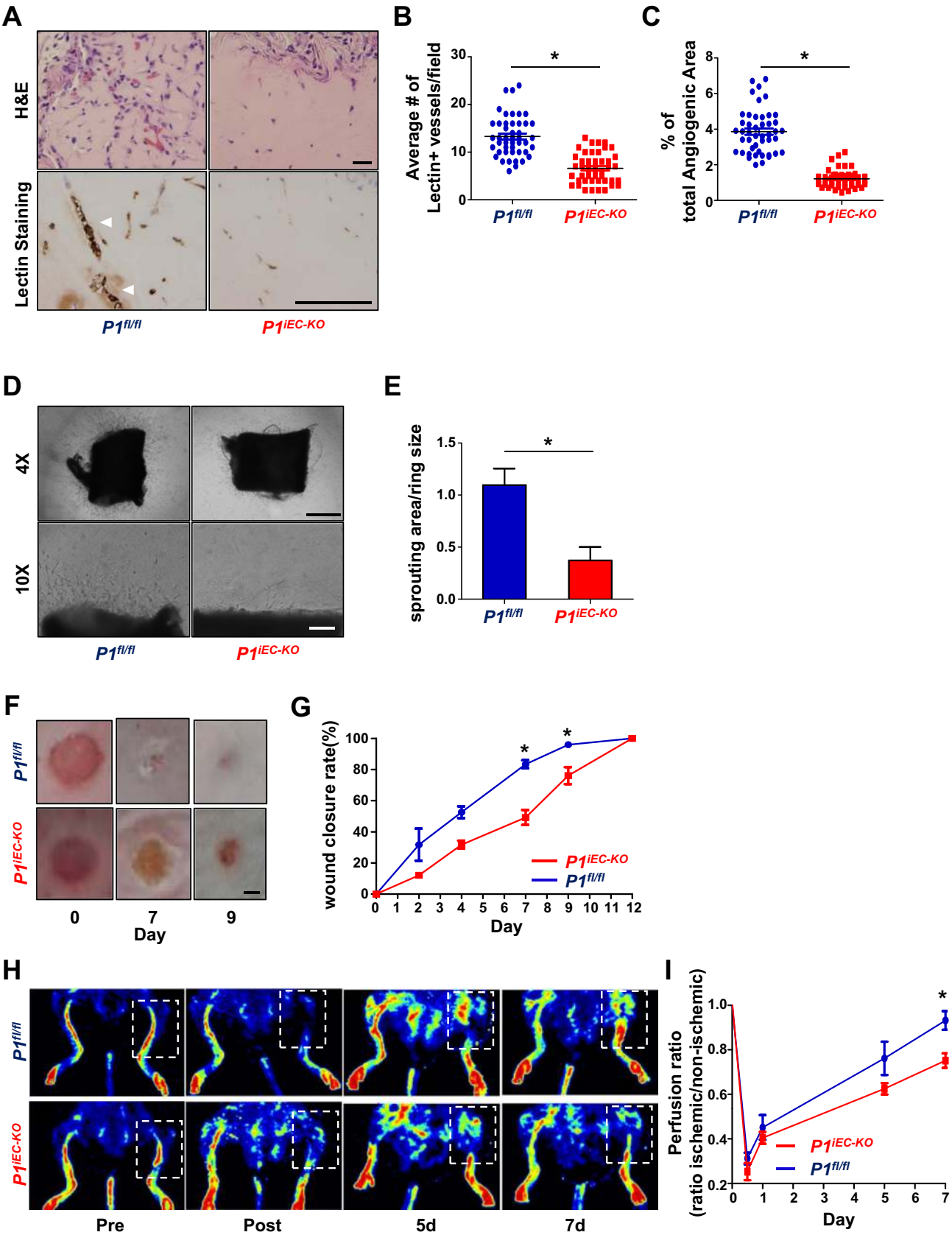

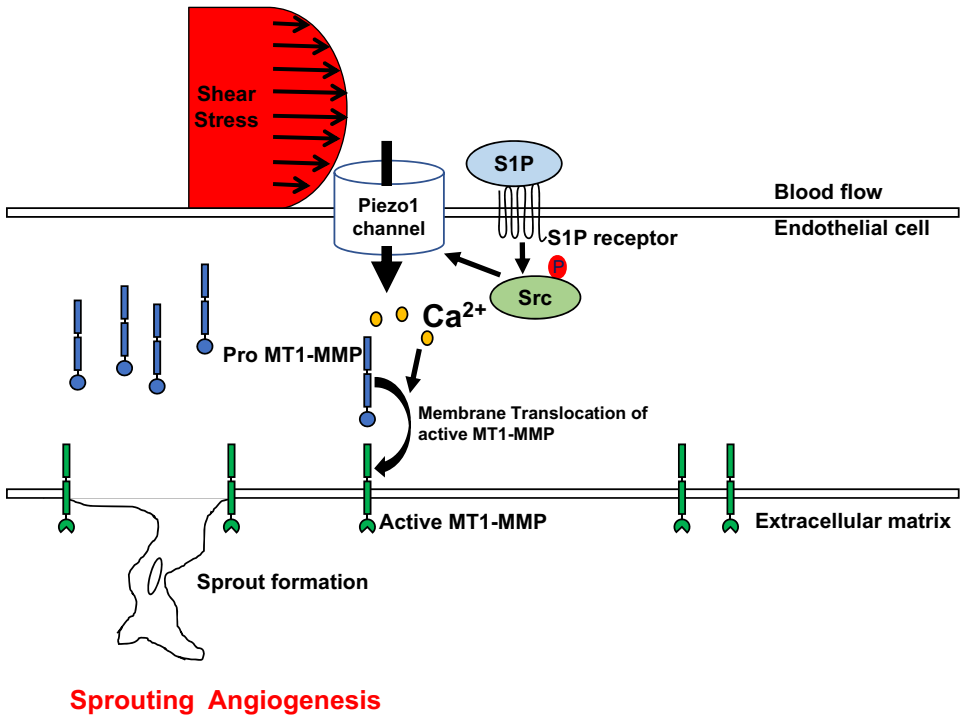

Fig. 7. Schematic model showing that wall shear stress/sphingosine 1-phosphate (WSS/S1P) activates Piezo1, which induces required Ca^{2+} gating and membrane type 1 matrix metalloproteinase-1 (MT1-MMP) signaling and thereby mediates sprouting angiogenesis.

Piezo1 in wound healing, which is dependent on angiogenesis (38). In a murine model of wound healing, we observed that $P1^{iEC\text{-}KO}$ mice displayed significantly delayed wound closure compared with $P1^{fl/fl}$ mice (Fig. 6, *F* and *G*). The wound was fully healed on *day 9* in $P1^{fl/fl}$ mice and on *day 12* in $P1^{iEC\text{-}KO}$ mice. These findings suggest that Piezo1 deletion in endothelial cells inhibits wound angiogenesis.

To further verify the important role of Piezo1 in promoting angiogenesis, we also used the mouse model of hindlimb ischemia (37). $P1^{fl/fl}$ and $P1^{iEC\text{-}KO}$ mice were subjected to unilateral hindlimb ischemia. Laser Doppler blood flow measurements demonstrated that hindlimb blood flow was markedly reduced compared with the nonischemic controls in $P1^{fl/fl}$ and $P1^{iEC\text{-}KO}$ mice 7 days after femoral artery ligation (Fig. 6*H*). However, the blood flow recovery after ischemia was significantly delayed in $P1^{iEC\text{-}KO}$ mice compared with $P1^{fl/fl}$ mice (Fig. 6*I*).

DISCUSSION

This study reveals a novel regulatory role for the mechanosensitive ion channel Piezo1 in sprouting angiogenesis. Both WSS and S1P stimulated Piezo1-mediated Ca^{2+} influx, which regulated MMP2 activation and MT1-MMP plasma membrane translocation to promote endothelial invasion of 3D collagen matrix. Our data support the possibility that Piezo1 coordinates matrix proteolysis events during sprouting angiogenesis. We propose that a common Piezo1 angiogenic signaling underlies responses not only to mechanical stimuli but also to the proangiogenic mediator S1P.

Piezo1 is a mechanosensor controlling development of normal vascular architecture through regulation of Ca^{2+} entry (31). In the present study, we highlighted the importance of Piezo1 in angiogenesis in response to both mechanical and biochemical stimuli. In 3D collagen matrix studies, depletion of Piezo1 by specific siRNAs strongly suppressed sprout formation in the sprouts following WSS/S1P treatment. A spider toxin blocker of Piezo1 channels, GsMTx4, had a similar inhibitory effect on sprout formation as Piezo1 depletion, whereas Yoda1, a selective Piezo1 activator, mimicked WSS/S1P-induced sprouting responses in ECs. In the in vivo Matrigel plug experiments, addition of S1P induced robust angiogenesis in control $P1^{fl/fl}$ mice but failed when Piezo1 was deleted in ECs in $P1^{iEC\text{-}KO}$ mice. Furthermore, $P1^{iEC\text{-}KO}$ mice exhibited significantly delayed wound closure in the presence of S1P compared with that in $P1^{fl/fl}$ mice. Importantly, blood

Fig. 6. Angiogenesis is impaired in Piezo1 knockout mice. *A–C*: endothelial cell (EC)-specific deletion of Piezo1 ($P1^{iEC\text{-}KO}$) mice showed reduced vessel formation and angiogenesis. *A, top*: histology of Matrigel plugs by hematoxylin-eosin H&E) staining; *bottom*: micrographs showing representative images of Matrigel plug isolated from control and $P1^{iEC\text{-}KO}$ mice after 14 days of implantation. ECs of Matrigel implants were labeled with isolectin B4 (brown). $Piezo1^{flox/flox}$ ($P1^{fl/fl}$) and $P1^{iEC\text{-}KO}$ mice were injected subcutaneously with Matrigel plugs supplemented with sphingosine 1-phosphate (S1P; 2 μM). Scale bar, 100 μm. Scatter dot graph shows mean number of newly formed B4+ vessels (*B*) and %total angiogenic area (*C*) in Matrigel plugs; $n = 5$ mice per group (46 fields each). $^*P < 0.05$, Student's *t*-test. *D* and *E*: $P1^{iEC\text{-}KO}$ mice exhibited impaired vessel sprouting and tube elongation. Aortic rings (1 mm diameter) were cultured in rat tail collagen type I matrix supplemented with 1 μM S1P for 4 days. *D*: representative micrographs of each arm of the experiment are shown. Scale bars, 500 μm (*top*) and 200 μm (*bottom*). *E*: statistical morphometric analysis of sprouting area of 4 mice/group from *D*; $n = 10$ aortic rings/group. $^*P < 0.05$, Student's *t*-test. *F* and *G*: $P1^{iEC\text{-}KO}$ mice showed delayed wound healing. *F*: representative image of cutaneous wounds (3 mm in diameter). *G*: wound closure rate (*right*) from *F*. Scale bar, 1 mm; $n = 4$ mice per group. $^*P < 0.05$, Student's *t*-test. *H* and *I*: impaired postischemic neovascularization in $P1^{iEC\text{-}KO}$ mice. *H*: representative perfusion images at 0, 1, 5, and 7 days measured by laser Doppler. *I*: blood flow recovery after hindlimb ischemia in $P1^{fl/fl}$ and $P1^{iEC\text{-}KO}$ mice shown as ratio of laser Doppler-measured perfusion values of ischemic (*left*) and nonischemic (*right*) legs; $n = 6$ mice per group. $^*P < 0.05$, Student's *t*-test.

flow recovery after ischemia in hindlimbs was significantly reduced in $P1^{iEC\text{-}KO}$ mice compared with $P1^{fl/fl}$ mice. These findings establish an essential role for endothelial Piezo1 in the pathophysiology of angiogenesis and identify Piezo1 as a novel therapeutic target for sprouting angiogenesis.

We (20) have previously shown that neither WSS at 5 dyne/cm^2 nor S1P (1 μM) alone induced sprouting angiogenesis, but when combined, the response was greatly amplified. Our current results clearly support the notion that the synergism between WSS and S1P was the result of activation of the gating of Ca^{2+} via Piezo1. WSS is experienced at the endothelial luminal surface during vascular development and in vascularized tumors (11, 19, 32). The mechanosensitive Piezo1 is expressed in ECs (31) and responds to WSS (7, 31, 35). Piezo1 can be activated by increased membrane bilayer tension and change in membrane curvature (9, 10). Although Piezo1 is involved in various biological processes and can gate Ca^{2+} in response to mechanical stimuli (9, 29, 31), its state of activation at the ambient WSS in venules is not sufficient to trigger angiogenesis. In this study, we have demonstrated the requisite role of S1P signaling in activating the Ca^{2+} gating function of Piezo1, which mediated sprouting angiogenesis. The S1P-activated signaling cascade was essential for the optimal gating Ca^{2+} via Piezo1 and rise in intracellular Ca^{2+} that thereby activated MT1-MMP signaling and the angiogenesis program. S1P signaling and WSS thus functioned synergistically in activating Piezo1-mediated Ca^{2+} entry. S1P is important in this context because it is released in micromolar concentrations by activated ECs and platelets in ischemic tissue (16, 42). These findings thus support the model that S1P activation of Piezo1 at WSS at 5 dyne/cm^2, the level approximating venular WSS, induces Ca^{2+} influx via Piezo1, which activates MT1-MMP to mediate angiogenesis. Piezo1 activation may thus be an important mechanism of sprouting angiogenesis in venules in the context of generation of S1P in the local ischemic milieu.

The mechanism by which S1P activates Piezo1 is not clear. We identified that c-Src was required for activation of Piezo1 Ca^{2+} signaling and thereby sprouting angiogenesis. This was clearly evident in studies in which constitutive activation of Src family kinases by exogenous expression of the RapR-Src construct (5) directly induced Ca^{2+} entry via Piezo1. How Src activation stimulates Piezo1 signaling remains unknown. Piezo1 phosphorylation at Ser^{1621} and Thr^{1626} sites has been previously identified (46). It is likely that Src induces gating via Piezo1 through a phosphorylation step and change in the channel conformation to allow Ca^{2+} influx. Piezo1-mediated Ca^{2+} influx downstream of S1P signaling was clearly consequential. We observed that the rise in intracellular Ca^{2+} caused by Piezo1 activation was a trigger for activation and membrane translocation of MT1-MMP, which are essential for remodeling extracellular matrix and mediating angiogenesis (6, 39). The MT1-MMP cytoplasmic tail is also directly phosphorylated by Src to regulate proteolytic activity and membrane localization (28). Therefore, S1P and WSS synergistically stimulated translocation of MT1-MMP to the membrane through Piezo1-mediated Ca^{2+} influx (22).

Increased WSS is a common feature of vascular diseases with perturbed hemodynamics (4) and rapidly growing vessels of aggressive tumors (19). Piezo1 expression has been found to increase in a variety of cancers (30, 43). Piezo1 is highly expressed in human breast cancer cell line MCF-7 cells and the Piezo1 inhibitor GsMTx4 inhibited the motility of MCF-7 (30). Knockdown of Piezo1 in gastric tumor cell lines was associated with decreased cell migration (43). Thus, we surmise that blocking Ca^{2+} influx via inhibition of Piezo1 may be an attractive anti-cancer strategy.

In summary, our results strongly suggest that Piezo1 mediates sprouting angiogenesis caused by WSS and S1P treatment. It is important to note that mechanical and biochemical stimuli share a common signaling Piezo1-mediated Ca^{2+} influx, which causes activation and membrane translocation of MT1-MMP and subsequent sprouting angiogenesis (Fig. 7). These findings open the door to new therapeutic strategies for a broad range of angiogenesis-related diseases such as cancer, ischemic heart disease, and atherosclerosis on the basis of modulation of Piezo1 activation.

ACKNOWLEDGMENTS

We thank Dr. David J. Beech for the $Piezo1^{flox/flox}$ mice.

Present address of A. B. Malik: Department of Pharmacology, Univ. of Illinois College of Medicine, E403 MSB 835 S. Wolcott Ave., Chicago, IL 60612 (Tel: 312-996-7636; e-mail: abmalik@uic.edu).

GRANTS

This work was supported in part by American Heart Association Scientist Development Grant 17SDG33700146 to H. Kang and by National Heart, Lung, and Blood Institute Grants P01 HL-060678 to A. B. Malik and R01 HL-104092 to G. Hu.

DISCLOSURES

No conflicts of interest, financial or otherwise, are declared by the authors.

AUTHOR CONTRIBUTIONS

H.K., G.H., and A.B.M. conceived and designed research; H.K., Z.H., M.Z., and J.K. performed experiments; H.K., Z.H., M.Z., J.K., G.H., and A.B.M. analyzed data; H.K. and A.B.M. interpreted results of experiments; H.K. prepared figures; H.K. drafted manuscript; H.K., K.J.B., D.M., A.V.K., G.H., and A.B.M. edited and revised manuscript; G.H. and A.B.M. approved final version of manuscript.

REFERENCES

1. **Bae C, Gnanasambandam R, Nicolai C, Sachs F, Gottlieb PA.** Xerocytosis is caused by mutations that alter the kinetics of the mechanosensitive channel PIEZO1. *Proc Natl Acad Sci USA* 110: E1162–E1168, 2013. doi:10.1073/pnas.1219777110.
2. **Cahalan SM, Lukacs V, Ranade SS, Chien S, Bandell M, Patapoutian A.** Piezo1 links mechanical forces to red blood cell volume. *eLife* 4: e07370, 2015. doi:10.7554/eLife.07370.
3. **Carmeliet P, Jain RK.** Angiogenesis in cancer and other diseases. *Nature* 407: 249–257, 2000. doi:10.1038/35025220.
4. **Chiu J-J, Chien S.** Effects of disturbed flow on vascular endothelium: pathophysiological basis and clinical perspectives. *Physiol Rev* 91: 327–387, 2011. doi:10.1152/physrev.00047.2009.
5. **Chu P-H, Tsygankov D, Berginski ME, Dagliyan O, Gomez SM, Elston TC, Karginov AV, Hahn KM.** Engineered kinase activation reveals unique morphodynamic phenotypes and associated trafficking for Src family isoforms. *Proc Natl Acad Sci USA* 111: 12420–12425, 2014. doi:10.1073/pnas.1404487111.
6. **Chun T-H, Sabeh F, Ota I, Murphy H, McDonagh KT, Holmbeck K, Birkedal-Hansen H, Allen ED, Weiss SJ.** MT1-MMP-dependent neovessel formation within the confines of the three-dimensional extracellular matrix. *J Cell Biol* 167: 757–767, 2004. doi:10.1083/jcb.200405001.
7. **Cinar E, Zhou S, DeCourcey J, Wang Y, Waugh RE, Wan J.** Piezo1 regulates mechanotransductive release of ATP from human RBCs. *Proc Natl Acad Sci USA* 112: 11783–11788, 2015. doi:10.1073/pnas.1507309112.
8. **Clark ER.** Studies on the growth of blood vessels in the tail of the frog larva - by observation and experiment on the living animal. *Am J Anat* 23: 37–88, 1918. doi:10.1002/aja.1000230103.

9. **Coste B, Murthy SE, Mathur J, Schmidt M, Mechioukhi Y, Delmas P, Patapoutian A.** Piezo1 ion channel pore properties are dictated by C-terminal region. *Nat Commun* 6: 7223, 2015. doi:10.1038/ncomms8223.
10. **Cox CD, Bae C, Ziegler L, Hartley S, Nikolova-Krstevski V, Rohde PR, Ng C-A, Sachs F, Gottlieb PA, Martinac B.** Removal of the mechanoprotective influence of the cytoskeleton reveals PIEZO1 is gated by bilayer tension. *Nat Commun* 7: 10366, 2016. doi:10.1038/ncomms10366.
11. **Culver JC, Dickinson ME.** The effects of hemodynamic force on embryonic development. *Microcirculation* 17: 164–178, 2010. doi:10.1111/j.1549-8719.2010.00025.x.
12. **Gadepalli VS, Vaughan C, Rao RR.** Isolation and characterization of murine multipotent lung stem cells. *Methods Mol Biol* 962: 183–191, 2013. doi:10.1007/978-1-62703-236-0_15.
13. **Ge J, Li W, Zhao Q, Li N, Chen M, Zhi P, Li R, Gao N, Xiao B, Yang M.** Architecture of the mammalian mechanosensitive Piezo1 channel. *Nature* 527: 64–69, 2015. doi:10.1038/nature15247.
14. **Gerhardt H.** VEGF and endothelial guidance in angiogenic sprouting. *Organogenesis* 4: 241–246, 2008. doi:10.4161/org.4.4.7414.
15. **Göthert JR, Gustin SE, van Eekelen JAM, Schmidt U, Hall MA, Jane SM, Green AR, Göttgens B, Izon DJ, Begley CG.** Genetically tagging endothelial cells in vivo: bone marrow-derived cells do not contribute to tumor endothelium. *Blood* 104: 1769–1777, 2004. doi:10.1182/blood-2003-11-3952.
16. **Ham A, Kim M, Kim JY, Brown KM, Fruttiger M, D'Agati VD, Lee HT.** Selective deletion of the endothelial sphingosine-1-phosphate 1 receptor exacerbates kidney ischemia-reperfusion injury. *Kidney Int* 85: 807–823, 2014. doi:10.1038/ki.2013.345.
17. **Hernández Vera R, Genové E, Alvarez L, Borrós S, Kamm R, Lauffenburger D, Semino CE.** Interstitial fluid flow intensity modulates endothelial sprouting in restricted Src-activated cell clusters during capillary morphogenesis. *Tissue Eng Part A* 15: 175–185, 2009. doi:10.1089/ten.tea.2007.0314.
18. **Ichioka S, Shibata M, Kosaki K, Sato Y, Harii K, Kamiya A.** Effects of shear stress on wound-healing angiogenesis in the rabbit ear chamber. *J Surg Res* 72: 29–35, 1997. doi:10.1006/jsre.1997.5170.
19. **Jain RK, Martin JD, Stylianopoulos T.** The role of mechanical forces in tumor growth and therapy. *Annu Rev Biomed Eng* 16: 321–346, 2014. doi:10.1146/annurev-bioeng-071813-105259.
20. **Kang H, Bayless KJ, Kaunas R.** Fluid shear stress modulates endothelial cell invasion into three-dimensional collagen matrices. *Am J Physiol Heart Circ Physiol* 295: H2087–H2097, 2008. doi:10.1152/ajpheart.00281.2008.
21. **Kang H, Duran CL, Abbey CA, Kaunas RR, Bayless KJ.** Fluid shear stress promotes proprotein convertase-dependent activation of MT1-MMP. *Biochem Biophys Res Commun* 460: 596–602, 2015. doi:10.1016/j.bbrc.2015.03.075.
22. **Kang H, Kwak HI, Kaunas R, Bayless KJ.** Fluid shear stress and sphingosine 1-phosphate activate calpain to promote membrane type 1 matrix metalloproteinase (MT1-MMP) membrane translocation and endothelial invasion into three-dimensional collagen matrices. *J Biol Chem* 286: 42017–42026, 2011. doi:10.1074/jbc.M111.290841.
23. **Kaunas R, Kang H, Bayless KJ.** Synergistic regulation of angiogenic sprouting by biochemical factors and wall shear stress. *Cell Mol Bioeng* 4: 547–559, 2011. doi:10.1007/s12195-011-0208-5.
24. **Kessenbrock K, Plaks V, Werb Z.** Matrix metalloproteinases: regulators of the tumor microenvironment. *Cell* 141: 52–67, 2010. doi:10.1016/j.cell.2010.03.015.
25. **Kim MB, Sarelius IH.** Distributions of wall shear stress in venular convergences of mouse cremaster muscle. *Microcirculation* 10: 167–178, 2003. doi:10.1080/713773612.
26. **Koutsiaris AG, Tachmitzi SV, Batis N, Kotoula MG, Karabatsas CH, Tsironi E, Chatzoulis DZ.** Volume flow and wall shear stress quantification in the human conjunctival capillaries and post-capillary venules in vivo. *Biorheology* 44: 375–386, 2007.
27. **Kwak HI, Kang H, Dave JM, Mendoza EA, Su SC, Maxwell SA, Bayless KJ.** Calpain-mediated vimentin cleavage occurs upstream of MT1-MMP membrane translocation to facilitate endothelial sprout initiation. *Angiogenesis* 15: 287–303, 2012. doi:10.1007/s10456-012-9262-4.
28. **Langlois S, Nyalendo C, Di Tomasso G, Labrecque L, Roghi C, Murphy G, Gingras D, Béliveau R.** Membrane-type 1 matrix metalloproteinase stimulates cell migration through epidermal growth factor receptor transactivation. *Mol Cancer Res* 5: 569–583, 2007. doi:10.1158/1541-7786.MCR-06-0267.
29. **Lewis AH, Grandl J.** Mechanical sensitivity of Piezo1 ion channels can be tuned by cellular membrane tension. *eLife* 4: e12088, 2015. doi:10.7554/eLife.12088.
30. **Li C, Rezania S, Kammerer S, Sokolowski A, Devaney T, Gorischek A, Jahn S, Hackl H, Groschner K, Windpassinger C, Malle E, Bauernhofer T, Schreibmayer W.** Piezo1 forms mechanosensitive ion channels in the human MCF-7 breast cancer cell line. *Sci Rep* 5: 8364, 2015. doi:10.1038/srep08364.
31. **Li J, Hou B, Tumova S, Muraki K, Bruns A, Ludlow MJ, Sedo A, Hyman AJ, McKeown L, Young RS, Yuldasheva NY, Majeed Y, Wilson LA, Rode B, Bailey MA, Kim HR, Fu Z, Carter DAL, Bilton J, Imrie H, Ajuh P, Dear TN, Cubbon RM, Kearney MT, Prasad RK, Evans PC, Ainscough JFX, Beech DJ.** Piezo1 integration of vascular architecture with physiological force. *Nature* 515: 279–282, 2014. doi:10.1038/nature13701.
32. **Lucitti JL, Jones EAV, Huang C, Chen J, Fraser SE, Dickinson ME.** Vascular remodeling of the mouse yolk sac requires hemodynamic force. *Development* 134: 3317–3326, 2007. doi:10.1242/dev.02883.
33. **Marrotte EJ, Chen D-D, Hakim JS, Chen AF.** Manganese superoxide dismutase expression in endothelial progenitor cells accelerates wound healing in diabetic mice. *J Clin Invest* 120: 4207–4219, 2010. doi:10.1172/JCI36858.
34. **Pathak MM, Nourse JL, Tran T, Hwe J, Arulmoli J, Le DTT, Bernardis E, Flanagan LA, Tombola F.** Stretch-activated ion channel Piezo1 directs lineage choice in human neural stem cells. *Proc Natl Acad Sci USA* 111: 16148–16153, 2014. doi:10.1073/pnas.1409802111.
35. **Ranade SS, Qiu Z, Woo S-H, Hur SS, Murthy SE, Cahalan SM, Xu J, Mathur J, Bandell M, Coste B, Li Y-SJ, Chien S, Patapoutian A.** Piezo1, a mechanically activated ion channel, is required for vascular development in mice. *Proc Natl Acad Sci USA* 111: 10347–10352, 2014. doi:10.1073/pnas.1409233111.
36. **Senger DR, Davis GE.** Angiogenesis. *Cold Spring Harb Perspect Biol* 3: a005090, 2011. doi:10.1101/cshperspect.a005090.
37. **Shireman PK, Quinones MP.** Differential necrosis despite similar perfusion in mouse strains after ischemia. *J Surg Res* 129: 242–250, 2005. doi:10.1016/j.jss.2005.06.013.
38. **Singer AJ, Clark RA.** Cutaneous wound healing. *N Engl J Med* 341: 738–746, 1999. doi:10.1056/NEJM199909023411006.
39. **Stratman AN, Saunders WB, Sacharidou A, Koh W, Fisher KE, Zawieja DC, Davis MJ, Davis GE.** Endothelial cell lumen and vascular guidance tunnel formation requires MT1-MMP-dependent proteolysis in 3-dimensional collagen matrices. *Blood* 114: 237–247, 2009. doi:10.1182/blood-2008-12-196451.
40. **Syeda R, Xu J, Dubin AE, Coste B, Mathur J, Huynh T, Matzen J, Lao J, Tully DC, Engels IH, Petrassi HM, Schumacher AM, Montal M, Bandell M, Patapoutian A.** Chemical activation of the mechanotransduction channel Piezo1. *eLife* 4: e07369, 2015. doi:10.7554/eLife.07369.
41. **Walter DH, Rochwalsky U, Reinhold J, Seeger F, Aicher A, Urbich C, Spyridopoulos I, Chun J, Brinkmann V, Keul P, Levkau B, Zeiher AM, Dimmeler S, Haendeler J.** Sphingosine-1-phosphate stimulates the functional capacity of progenitor cells by activation of the CXCR4-dependent signaling pathway via the S1P3 receptor. *Arterioscler Thromb Vasc Biol* 27: 275–282, 2007. doi:10.1161/01.ATV.0000254669.12675.70.
42. **Won Park SW, Kim M, Brown KM, D'Agati VD, Lee HT.** Inhibition of sphingosine 1-phosphate receptor 2 protects against renal ischemia-reperfusion injury. *J Am Soc Nephrol* 23: 266–280, 2012. doi:10.1681/ASN.2011050503.
43. **Yang XN, Lu YP, Liu JJ, Huang JK, Liu YP, Xiao CX, Jazag A, Ren JL, Guleng B.** Piezo1 is as a novel trefoil factor family 1 binding protein that promotes gastric cancer cell mobility in vitro. *Dig Dis Sci* 59: 1428–1435, 2014. doi:10.1007/s10620-014-3044-3.
44. **Zhou Z, Apte SS, Soininen R, Cao R, Baaklini GY, Rauser RW, Wang J, Cao Y, Tryggvason K.** Impaired endochondral ossification and angiogenesis in mice deficient in membrane-type matrix metalloproteinase I. *Proc Natl Acad Sci USA* 97: 4052–4057, 2000. doi:10.1073/pnas.060037197.
45. **Zimnicka AM, Husain YS, Shajahan AN, Sverdlov M, Chaga O, Chen Z, Toth PT, Klomp J, Karginov AV, Tiruppathi C, Malik AB, Minshall RD.** Src-dependent phosphorylation of caveolin-1 Tyr-14 promotes swelling and release of caveolae. *Mol Biol Cell* 27: 2090–2106, 2016. doi:10.1091/mbc.e15-11-0756.
46. **Zuccala ES, Satchwell TJ, Angrisano F, Tan YH, Wilson MC, Heesom KJ, Baum J.** Quantitative phospho-proteomics reveals the Plasmodium merozoite triggers pre-invasion host kinase modification of the red cell cytoskeleton. *Sci Rep* 6: 19766, 2016. doi:10.1038/srep19766.